NASA TECHNICAL NOTE

NASA TN D-2283

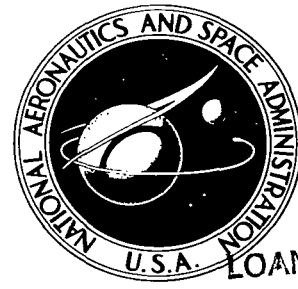

NASA TN D-2283

A STUDY OF THE STABILITY AND LOCATION OF THE CENTER OF PRESSURE ON SHARP, RIGHT CIRCULAR CONES AT HYPERSONIC SPEEDS

by Jim A. Penland

Langley Research Center
Langley Station, Hampton, Va.

NATIONAL AERONAUTICS AND SPACE ADMINISTRATION • WASHINGTON, D. C. • MAY 1964

A STUDY OF THE STABILITY AND LOCATION OF THE CENTER OF PRESSURE ON SHARP, RIGHT CIRCULAR CONES AT HYPERSONIC SPEEDS

By Jim A. Penland

Langley Research Center
Langley Station, Hampton, Va.

NATIONAL AERONAUTICS AND SPACE ADMINISTRATION

For sale by the Office of Technical Services, Department of Commerce,
Washington, D.C. 20230 -- Price $1.00

A STUDY OF THE STABILITY AND LOCATION OF THE CENTER OF PRESSURE ON SHARP, RIGHT CIRCULAR CONES AT HYPERSONIC SPEEDS

By Jim A. Penland
Langley Research Center

SUMMARY

Analysis of experimental data obtained on various sharp, right circular cone models at a Mach number of 6.8 and a Reynolds number of 0.22×10^6 per inch indicates that the Newtonian theory gives good predictions of the longitudinal stability and performance parameters through a 30° angle-of-attack range for cones with semivertex angles less than 40°. The location of the center of pressure was found to be fixed for a given cone angle and independent of angle-of-attack change. A decrease in Reynolds number by a factor of 5 made no change in the longitudinal characteristics of a 5° semivertex cone except an increase of drag due to skin friction.

The calculated longitudinal characteristics are presented for cones with semivertex angles of 2.5° to 50° in Newtonian flow for angles of attack from 0° to 180° with both base area and planform area reference.

INTRODUCTION

The initial design of a missile or reentry configuration requires a knowledge of the stability, the center-of-pressure location, and the associated variations of these parameters with any change of configuration, angle of attack, or Reynolds number. These data are necessary in order to determine the optimum center-of-moment location, to determine any necessary control surfaces or forces, and to calculate flight trajectories.

One of the many aerodynamic shapes undergoing tests is the simple conical body.

Considerable force and pressure-distribution data are available on sharp cones at supersonic and hypersonic speeds (refs. 1 to 17); however, few pitching-moment data are available except for cones of small semivertex angle.

The purpose of this investigation was to determine at hypersonic speeds the variation of pitching moment and the location of the center of pressure of

sharp cones having semivertex angles of 5° to 50° through an angle-of-attack range of -5° to 30° and to compare the results with available hypersonic data in air and helium and Newtonian theory.

SYMBOLS

$C = \frac{\mu_w T_\infty}{\mu_\infty T_w} = 0.86$

C_A axial-force coefficient, $\frac{(F_A - F_b)}{q_\infty S_b}$

C_D drag coefficient, $\frac{F_D'}{q_\infty S_b}$

C_F average skin-friction coefficient, $\frac{1.328\sqrt{C}}{\sqrt{R_l}} \frac{2\sqrt{3}}{3} \frac{S_s q_l}{S_b q_\infty}$

C_L lift coefficient, $\frac{F_L}{q_\infty S_b}$

C_m pitching-moment coefficient, $\frac{M}{q_\infty S_b L}$

C_{m_α} pitching-moment slope, $\left(\frac{\partial C_m}{\partial \alpha}\right)_{\alpha=0°}$

C_N normal-force coefficient, $\frac{F_N}{q_\infty S_b}$

$C_{p,max}$ maximum or stagnation pressure coefficient

D model base diameter

F_A axial force along X-axis; positive direction, -X

F_b base-pressure correction, $(p_\infty - p_b)S_b$

$F_D' = F_N \sin \alpha + F_A \cos \alpha - F_b \cos \alpha$

$F_L = F_N \cos \alpha - F_A \sin \alpha + F_b \sin \alpha$

F_N	normal force along Z-axis; positive direction, -Z
L	model length
L/D	lift-drag ratio, C_L/C_D
M	Mach number
p	static pressure
q	dynamic pressure
R	Reynolds number
S_b	base area of model
S_s	total surface area, excluding base area
T	temperature
x_{cm}	distance from model nose to center-of-moment location
x_{cp}	distance from model nose to center-of-pressure location
X,Z	body axes
α	angle of attack, deg
θ	semivertex angle of cone, deg
μ	dynamic viscosity

Subscripts:

∞	free-stream conditions
l	local conditions
w	wall conditions
b	model base

MODEL DESIGN PHILOSOPHY

A photograph of the models used during the present tests is shown as figure 1, and the geometric details are given in figure 2. The size of each model was determined by either the size of the tunnel-flow test area (approximately 6 × 6 inches), or the maximum model size that would allow the tunnel flow to

start. Starting of the hypersonic tunnel used during the present tests is assured if the maximum model size is such that its drag coefficient is equal to, or less than, that of a disk with a diameter of 2.87 inches, which is the maximum size of disk that will allow flow to start. The low-drag models were dimensioned to remain within the flow test area at $\alpha = 30^{\circ}$. All models were constructed of aluminum and were bored out internally to reduce the overall weights and thus the initial tare load interactions of the strain-gage balances. Based on the good correlation between the experimental and calculated normal forces and pitching moments in references 13 and 15, model centers of pressure determined by Newtonian theory were carefully located with respect to the balance moment center. With the model located on the balance in this manner, a minimum of pitching moment may be expected on the balance during tests; therefore, all forces and moments would be measured with greater accuracy because of further reduction of balance interactions.

APPARATUS AND TESTS

The tests were conducted in the Mach number 6.86 test section of the Langley 11-inch hypersonic tunnel. The tunnel-wall boundary-layer thickness and hence the free-stream Mach number of this test section are dependent upon the stagnation pressure. For these tests, the average stagnation pressure was 20 atmospheres and the average stagnation temperature 675° F (to avoid liquefaction). These conditions resulted in an average free-stream Mach number of 6.80 and an average unit Reynolds number of 0.220×10^{6} per inch. The absolute humidity was kept to less than 1.9×10^{-5} pound of water per pound of dry air for all tests.

In order to assure the best stability results obtainable with present-day methods, several precautions were taken during these tests. Three strain-gage balances were selected for the various models in order that the normal and axial components would be loaded near maximum through the -3° to 30° angle-of-attack range. To obtain greater accuracy near $\alpha = 0^{\circ}$, a second test was made of each model through an angle-of-attack range of -5° to 4° by using the more sensitive beams of the balance designed for side force and yawing moment and yawing the model in the tunnel-flow test region. This method minimized both initial tare loads and attitude tare loads, and thus produced data with a bare minimum of corrections between recorded outputs and final coefficients. The outputs from the various strain gages were continuously recorded on pen-marked strip-chart self-balancing potentiometers and thus gave a positive indication of a settling out period and any zero shifts due to aerodynamic heating. Balances were check loaded before and after tests to assure consistent calibration. With the exception of the tests at low Reynolds number, the tunnel operating pressures were set to give maximum blowdown running time; which allowed the maximum settling out time for each data point.

The model base pressures were measured at three positions in the plane of the angle of attack for all tests, and the axial-force component was adjusted by an average of these measurements to correspond to a base pressure equal to the free-stream static pressure. In all cases the base-pressure correction was

small as compared to the model axial force. The data were not corrected for pitching-moment increments produced by the pressure variation over the model bases, since these increments were found to be less than the accuracy of the balance read-out system.

PRECISION OF DATA

The maximum uncertainties in the measurement of the force and moment coefficients for the individual test points as a result of the inaccuracies in the force balance read-out system are presented as follows:

Model θ	$\alpha = -3^\circ$ to 30° test			$\alpha = -5^\circ$ to 4° test		
	C_N	C_A	C_m	C_N	C_A	C_m
5	±0.009	±0.006	±0.001	±0.003	±0.006	±0.0005
10	±.007	±.003	±.001	±.002	±.003	±.0004
20	±.006	±.003	±.001	±.002	±.003	±.0006
30	±.006	±.006	±.002	±.002	±.006	±.001
40	±.003	±.008	±.002	±.002	±.008	±.001
50	±.002	±.007	±.002	±.002	±.007	±.001

The stagnation pressure was measured to an accuracy of ±1.5 inches of mercury, and the Mach number was known to ±0.01, so that an accuracy of free-stream dynamic pressure of ±0.03 pound per square inch resulted.

THEORETICAL CALCULATIONS

The calculation of the longitudinal characteristics of a variety of sharp cones was made by use of the Newtonian theory of references 13, 18, and 19 with $C_{p,max} = 2.00$ through an angle-of-attack range of 0° to 180°. The results of these calculations, which include the effect of the circular bases with no skin friction added, are presented in the appendix of this paper with the coefficients based on both planform area and base area.

The results of these calculations with skin friction included are also shown on the plots of experimental data. An approximation of the average skin-friction coefficient was made by use of the following equation:

$$C_F = \frac{1.328\sqrt{C}}{\sqrt{R_l}} \frac{2\sqrt{3}}{3} \frac{S_s q}{S_b q_\infty}$$

which was obtained from reference 20 and modified for cones with the Mangler transformation, as suggested in reference 21. For the tunnel conditions under

consideration, a constant value of C of 0.86 was taken. The Reynolds number used was calculated for conditions on the surface of the cone at an angle of attack of 0°. The skin friction estimated by this method was assumed to be constant with varying angle of attack.

It is of particular interest that references 13, 22, and 23 have shown that, when the contribution of axial force to pitching moment is considered for cones, the ratio of the equations for pitching moment and normal force reduce to a constant for any semivertex angle:

$$\frac{C_m}{C_N} = \frac{2}{3}\left(1 + \tan^2\theta\right)$$

Therefore, in Newtonian flow the center of pressure is independent of angle of attack for any fixed semivertex angle, and a plot of C_m as a function of C_N will result in a straight line.

PRESENTATION AND DISCUSSION OF RESULTS

The experimental results for tests in the -3° to 30° angle-of-attack range include lift, drag, lift-drag ratio, pitching moment, normal force, and axial force for the axis system shown in figure 3 are presented in figures 4 to 9. These data are shown plotted against angle of attack and cone semivertex angle, along with curves calculated by Newtonian theory plus skin friction, as described in the section entitled "Theoretical Calculations."

Effect of Skin Friction and Reynolds Number on Performance Characteristics

The magnitude of the skin friction and its effect on the lift-drag ratio may be seen in figure 4 for the 5° and 10° semivertex angle cones by a comparison of the viscid and inviscid curves. The inset supplementary plots of axial-force coefficient show in detail the angle-of-attack region up to 5°. It should be noted that the measured axial-force coefficients and, subsequently, the drag coefficients are higher than can be accounted for by the Newtonian theory. This is in part the result of not accounting for induced effects upon pressure and skin friction and the failure of Newtonian theory at low angles of attack. This underestimation, along with a complementary lower prediction of lift, accounts for the good estimation of lift-drag ratio, particularly for the cones of higher semivertex angle (i.e., $\theta > 20^\circ$), where the effect of skin friction is negligible. At $\alpha = 0^\circ$ the exact values of axial-force coefficient from Kopal (ref. 24) with skin friction added are given for all cones. With the exception of the 5° semivertex cone, for which the induced effects are large, nearly perfect prediction of axial force was made.

The results of tests on the 5° semivertex cone at two Reynolds numbers based on body length are also presented in figure 4. The plot of lift-drag ratio shows a decrease with a decrease in Reynolds number, as was expected from the increase in skin friction. A small variation of normal force may be noted in the negative angle-of-attack range, but the pitching moment was essentially unaffected by a Reynolds number change by a factor of 5. For the cone models having semivertex angles under 40° (figs. 4 and 5), the agreement between experiment and theory is good.

For the 40° and 50° cones (fig. 6) the axial force was considerably underpredicted at low angles of attack and overpredicted at the higher angles. This trend may be seen to exist for some of the less blunt cones. However, the angle of attack at which the crossover takes place (i.e., change from underprediction to overprediction) varies; it appears to decrease as the angle of the cone increases. This trend might be expected, inasmuch as Newtonian theory overpredicts the axial force of a 90° semivertex cone (flat plate) by about 15.5 percent at $\alpha = 0°$.

Longitudinal Stability Characteristics

The center of moments for all models was arbitrarily selected on the basis of a solid homogeneous cone with the center of gravity located at 75 percent of the body length. With this center-of-gravity location the 5° and 10° semivertex cones are unstable at angles of attack up to 30° but, due to a rearward movement of the center of pressure with increasing cone angle, the 20° cone is slightly stable and the 30° to 50° cones show considerable stability throughout the angle-of-attack range tested. The pitching moment was overpredicted for the 40° and 50° cones, but the predictions were excellent for cones with small semivertex angles. It may be concluded that the Newtonian theory for $C_{p,max} = 2.0$ gives excellent predictions of pitching moments with angle of attack for cones with semivertex angles under 40° through an angle-of-attack range up to 30°. This conclusion could also be drawn from the use of $C_{p,max} = 2.08$ which was derived by Lees (ref. 25) for unyawed cones at very high Mach numbers. The poor predictions of pitching moments for the 40° and 50° semivertex cones at the higher angles of attack are closely associated with the poor prediction of the axial force. As the lower half of the cone (below the line of symmetry) is most effective at these angles of attack, the overprediction of axial force means an overprediction of nose down, or negative, pitching moment due to axial force.

The variation of pitching moment with normal force is presented in figure 7. As discussed previously, the Newtonian theory predicts the ratio C_m/C_N to be a constant, dependent only on cone semivertex angle if the axial-force contribution to pitching moment is considered. For the angle-of-attack range up to 30° this appears to be nearly true for all cones tested. Only the 40° and 50° cones show a variation from the predicted straight-line curves, and this as a small difference in slope. The difference in the slope of the experimental-pitch—normal-force data and the theoretical curves indicates a variation in the location of the center of pressure. It should be noted that

no significant variation of parameter C_m/C_N was measured for the 5° semivertex cone during the variable Reynolds number tests.

Figure 8 presents a composite plot of available hypersonic data (refs. 13, 15, 16, 17, 26, and as yet unpublished data) in air and helium that shows the variation of the location of the experimental and theoretical center of pressure of cones with angle of attack and semivertex angle. The theoretical curves obtained from the previously mentioned relation $\frac{C_m}{C_N} = \frac{2}{3}\left(1 + \tan^2\theta\right)$ show that the center of pressure is located at the two-thirds body station for a cone having a semivertex angle of 0° and that it moves rearward so that it is located at the base (100 percent of body length) of a 35.3° cone and 61.8 percent of body length downstream of the base for a 50° cone. The center of pressure at $\alpha = 0°$ was obtained from the slope of the curves in figure 7 for the present data and from similar plots for the reference data. A comparison of the experimental data, both in air and in helium, with the Newtonian curves shows excellent agreement for cone semivertex angles up to about 30° and a trend of overprediction for the larger cone angles which increases with cone angle to about 10 percent of body length for a 50° cone. The experimental location of the center of pressure remains essentially fixed for any one model through the 60° angle-of-attack range, as predicted by the theory. It also appears that cone data obtained in air and helium at high Mach numbers are comparable.

The variation of the static stability parameter C_{m_α} at $\alpha = 0°$ is presented in figure 9 for various cone semivertex angles and center-of-moment locations. Experimental data are presented only for the center of moment at 75 percent of body length for the sake of clarity. For this center-of-moment location, a solid cone having a semivertex angle of about 19.4° would be neutrally stable. All cones show improved stability with increased semivertex angle. With the center of moment located at the cone base, that is, 100 percent of the body length, a cone having a semivertex angle of about 35.3° is neutrally stable, as mentioned in the discussion on center of pressure.

CONCLUDING REMARKS

Analysis of experimental data obtained on various sharp, right circular cone models at a Mach number of 6.8 and a Reynolds number of 0.22×10^6 per inch and a study of other hypersonic data in air and helium indicate that the Newtonian theory gives good predictions of the longitudinal stability and performance parameters through a 30° angle-of-attack range for cones with semivertex angles less than about 40°. Furthermore, it may be concluded that through a 60° angle-of-attack range the location of the center of pressure is essentially fixed for a given cone angle and is independent of angle-of-attack change, as predicted by Newtonian theory. Although a decrease of

Reynolds number by a factor of about 5 increased the axial force due to skin friction of a 5° semivertex angle cone by a factor of about 2.2, no effect upon stability or center of pressure was obtained.

Langley Research Center,
National Aeronautics and Space Administration,
Langley Station, Hampton, Va., January 7, 1964.

APPENDIX

NEWTONIAN FLOW ABOUT SHARP CIRCULAR CONES

An extensive set of calculations was made using Newtonian theory, as described in the section entitled "Theoretical Calculations." The results of these calculations are presented in figures 10 to 20 as a series of plots of the longitudinal characteristics of cones having semivertex angles of 2.5° to 50°. The coefficients shown in these figures include the effect of the forces on the flat circular bases at angles of attack greater than 90° and the effect of both normal and axial forces on pitching moment through the 0° to 180° angle-of-attack range. No skin friction was included in the calculations. Figures 10, 11, 13, 14, and 15 are presented with coefficients referenced to the planform area and figures 16 to 20 are presented with coefficients referenced to the base area. A stagnation pressure coefficient of 2.0 was used for all calculations.

REFERENCES

1. Cooper, Ralph D., and Robinson, Raymond A.: An Investigation of the Aerodynamic Characteristics of a Series of Cone-Cylinder Configurations at a Mach Number of 6.86. NACA RM L51J09, 1951.

2. Dennis, David H., and Cunningham, Bernard E.: Forces and Moments on Pointed and Blunt-Nosed Bodies of Revolution at Mach Numbers From 2.75 to 5.00. NACA RM A52E22, 1952.

3. Shantz, I.: Cone Static Stability Investigation at Mach Numbers 1.56 Through 4.24. NAVORD Rep. 3584, U.S. Naval Ord. Lab. (White Oak, Md.), Dec. 7, 1953. (Available as ASTIA Doc. AD 128203.)

4. Ridyard, Herbert W.: The Aerodynamic Characteristics of Two Series of Lifting Bodies at Mach Number 6.86. NACA RM L54C15, 1954.

5. Dennis, David H., and Cunningham, Bernard E.: Forces and Moments on Inclined Bodies at Mach Numbers From 3.0 to 6.3. NACA RM A54E03, 1954.

6. Oliver, Robert E.: An Experimental Investigation of Flow Over Simple Blunt Bodies at a Nominal Mach Number of 5.8. GALCIT Memo. No. 26 (Contract No. DA-04-495-Ord-19), June 1, 1955.

7. Liccini, L. L.: Hypersonic Tunnel No. 4 Results IX: The Development of a Water-Cooled Strain-Gage Balance (Including Sting Effects) and Its Application to a Study of Normal Force and Pitching Moments of a Cone and Cone-Cylinder at Mach Numbers 5 to 8. NAVORD Rep. 4334, U.S. Naval Ord. Lab. (White Oak, Md.), Aug. 20, 1956.

8. Lehnert, R., and Schermerhorn, V. L.: Wake Investigation on Sharp and Blunt Nose Cones at Supersonic Speeds. NAVORD Rep. 5668, U.S. Naval Ord. Lab. (White Oak, Md.), Jan. 28, 1958.

9. Maslach, G. J., and Talbot, L.: Low Density Aerodynamic Characteristics of a Cone at Angle of Attack. Tech. Rep. HE-150-172, Inst. Eng. Res., Univ. of California, Oct. 30, 1959.

10. Amick, James L.: Pressure Measurements on Sharp and Blunt 5°- and 15°-Half-Angle Cones at Mach Number 3.86 and Angles of Attack to 100°. NASA TN D-753, 1961.

11. Penland, Jim A.: Aerodynamic Force Characteristics of a Series of Lifting Cone and Cone-Cylinder Configurations at a Mach Number of 6.83 and Angles of Attack Up to 130°. NASA TN D-840, 1961.

12. Conti, Raul J.: Laminar Heat-Transfer and Pressure Measurements at a Mach Number of 6 on Sharp and Blunt 15° Half-Angle Cones at Angles of Attack up to 90°. NASA TN D-962, 1961.

13. Wells, William R., and Armstrong, William O.: Tables of Aerodynamic Coefficients Obtained From Developed Newtonian Expressions for Complete and Partial Conic and Spheric Bodies at Combined Angles of Attack and Sideslip With Some Comparisons With Hypersonic Experimental Data. NASA TR R-127, 1962.

14. Ladson, Charles L., and Blackstock, Thomas A. (with appendix by Donald L. Baradell and Thomas S. Blackstock): Air-Helium Simulation of the Aerodynamic Force Coefficients of Cones at Hypersonic Speeds. NASA TN D-1473, 1962.

15. Neal, Luther, Jr.: Aerodynamic Characteristics at a Mach Number of 6.77 of a 9° Cone Configuration, With and Without Spherical Afterbodies, at Angles of Attack Up to 180° With Various Degrees of Nose Blunting. NASA TN D-1606, 1963.

16. Whitfield, Jack D., and Wolny, W.: Correlation of Hypersonic Static-Stability Data From Blunt Slender Cones. AIAA Jour., vol. 1, no. 2, Feb. 1963, pp. 486-487.

17. Syvertson, Clarence A., and McDevitt, John B.: Effects of Mass Addition on the Stability of Slender Cones at Hypersonic Speeds. AIAA Jour., vol. 1, no. 4, Apr. 1963, pp. 939-940.

18. Grimminger, G., Williams, E. P., and Young, G. B. W.: Lift on Inclined Bodies of Revolution in Hypersonic Flow. Jour. Aero. Sci., vol. 17, no. 11, Nov. 1950, pp. 675-690.

19. Rainey, Robert W.: Working Charts for Rapid Prediction of Force and Pressure Coefficients on Arbitrary Bodies of Revolution by Use of Newtonian Concepts. NASA TN D-176, 1959.

20. Chapman, Dean R., and Rubesin, Morris W.: Temperature and Velocity Profiles in the Compressible Laminar Boundary Layer With Arbitrary Distribution of Surface Temperature. Jour. Aero. Sci., vol. 16, no. 9, Sept. 1949, pp. 547-565.

21. Eckert, Ernst R. G.: Survey on Heat Transfer at High Speeds. WADC Tech. Rep. 54-70, U.S. Air Force, Apr. 1954.

22. Charwat, A. F.: The Stability of Bodies of Revolution at Very High Mach Numbers. Jet Propulsion, vol. 27, no. 8, pt. 1, Aug. 1957, pp. 866-871.

23. Dugan, Duane W.: Estimation of Static Longitudinal Stability of Aircraft Configurations at High Mach Numbers and at Angles of Attack Between 0° and ±180°. NASA MEMO 1-17-59A, 1959.

24. Staff of Computing Section, Center of Analysis (Under Direction of Zdeněk Kopal): Tables of Supersonic Flow Around Cones. Tech. Rep. No. 1 (NOrd Contract No. 9169), M.I.T., 1947.

25. Lees, Lester: Hypersonic Flow. Fifth International Aeronautical Conference (Los Angeles, Calif., June 20-23, 1955), Inst. Aero. Sci., Inc., 1955, pp. 241-276.

26. Witcofski, Robert D., and Woods, William C.: Static Stability Characteristics of Blunt Low-Fineness-Ratio Bodies of Revolution at a Mach Number of 24.5 in Helium. NASA TN D-2282, 1964.

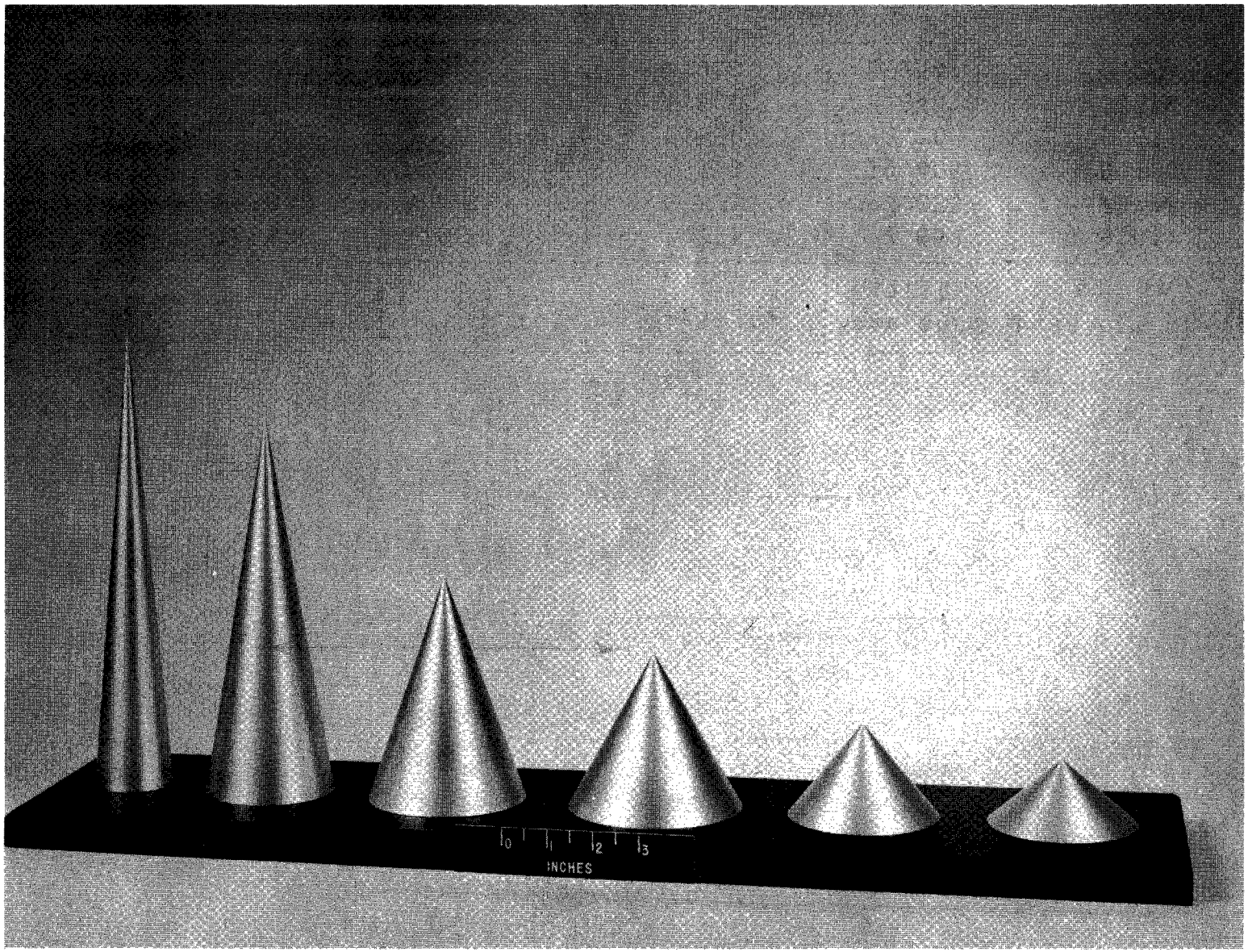

Figure 1.- Photograph of models tested. L-63-2110

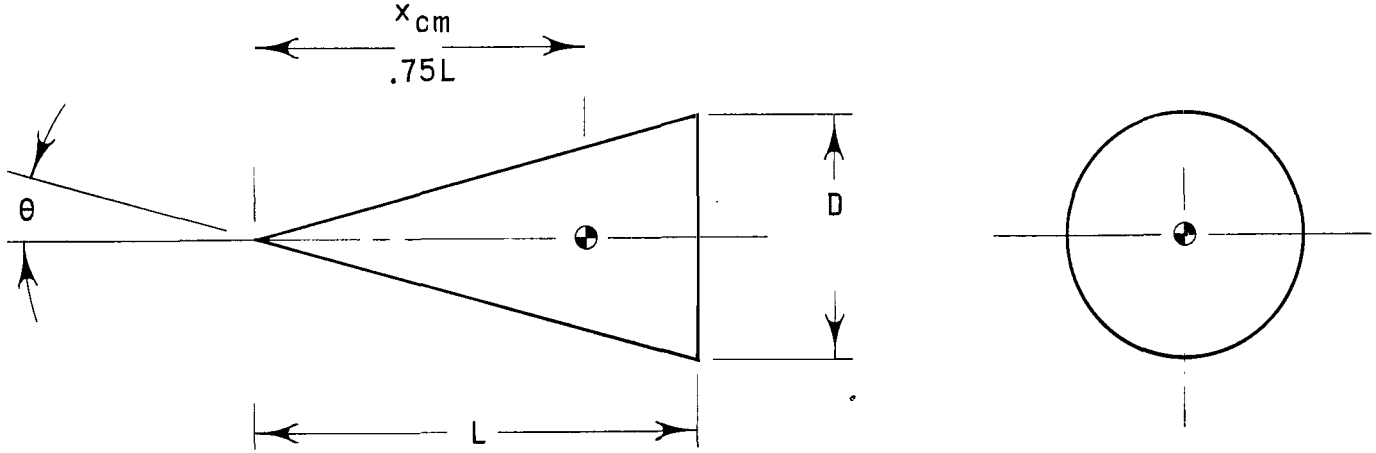

θ, deg	L, in.	D, in.	x_{cm}, in.	Base area, sq. in.	Planform area, sq. in
5	10.500	1.838	7.875	2.652	9.647
10	8.500	2.997	6.375	7.055	12.738
20	5.000	3.640	3.750	10.406	9.100
30	3.400	3.926	2.550	12.108	6.675
40	2.000	3.356	1.500	8.848	3.356
50	1.360	3.242	1.020	8.254	2.204

Figure 2.- Detail dimensions of models.

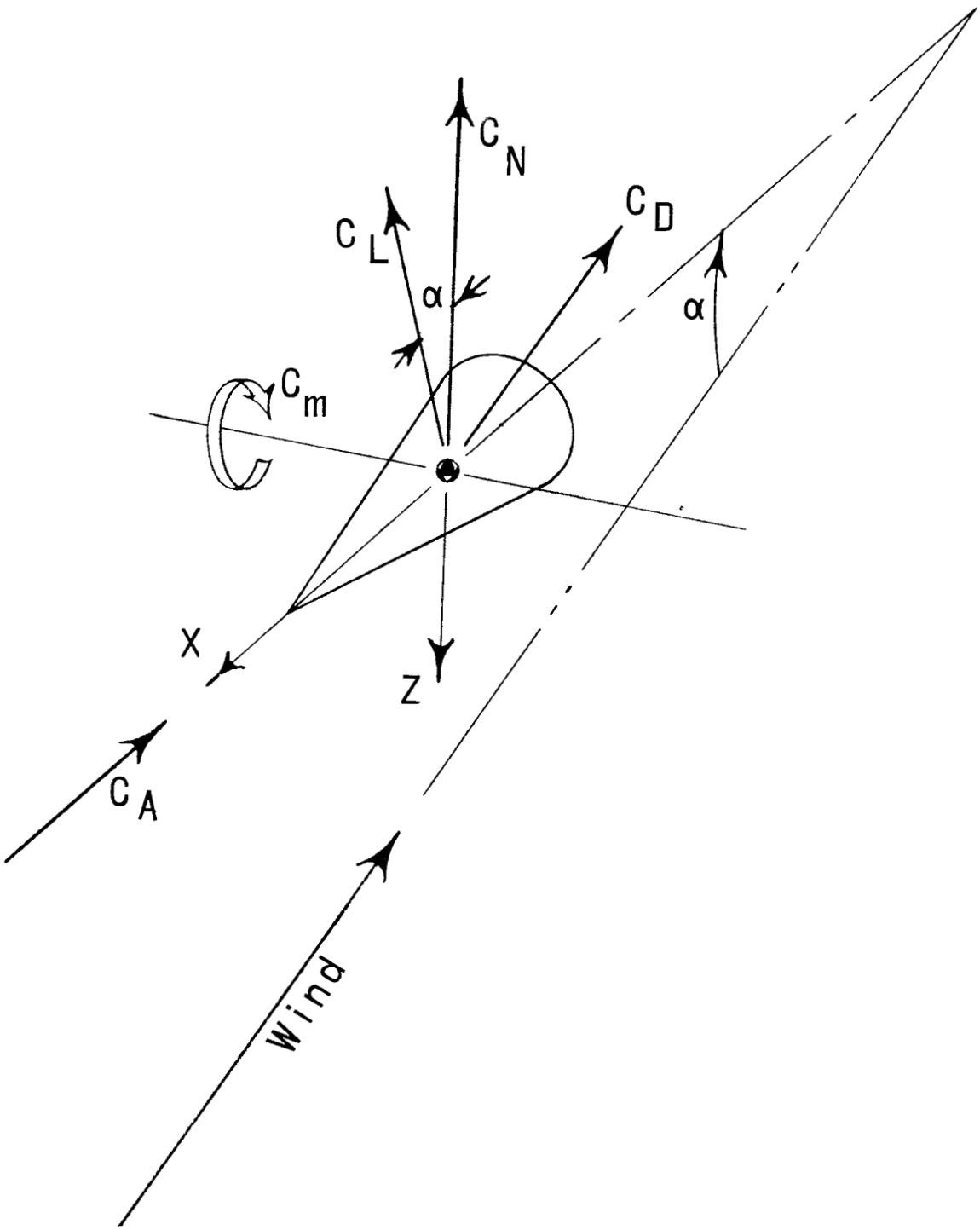

Figure 3.- Axis system. Arrows indicate positive direction.

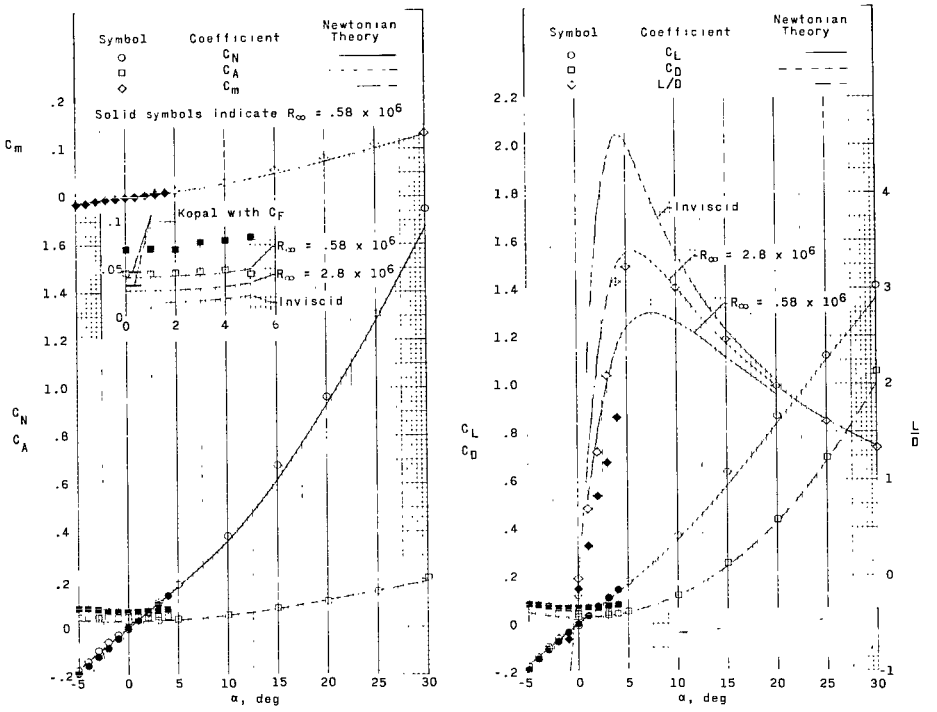

(a) $\theta = 5^\circ$; $R_\infty = 2.8 \times 10^6$.

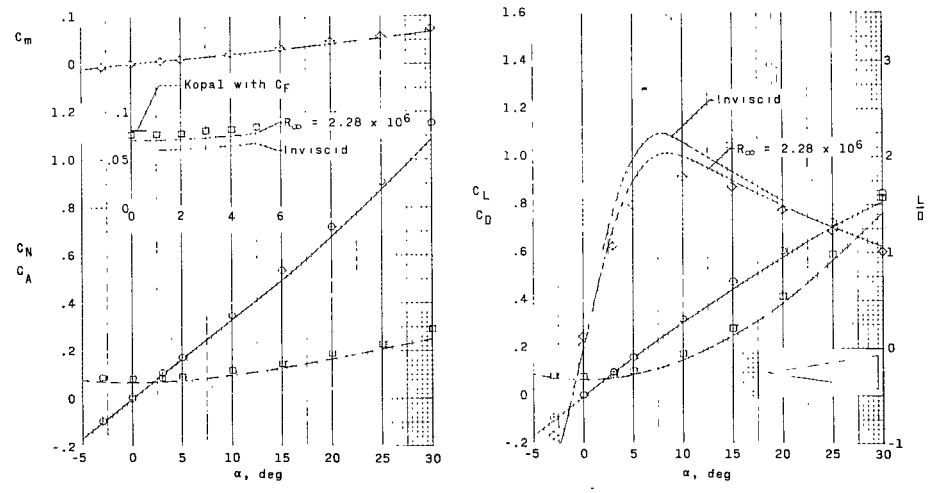

(b) $\theta = 10^\circ$; $R_\infty = 2.28 \times 10^6$.

Figure 4.- Comparison of longitudinal characteristics of cones having 5° and 10° semivertex angles with Newtonian theory. $M_\infty = 6.8$.

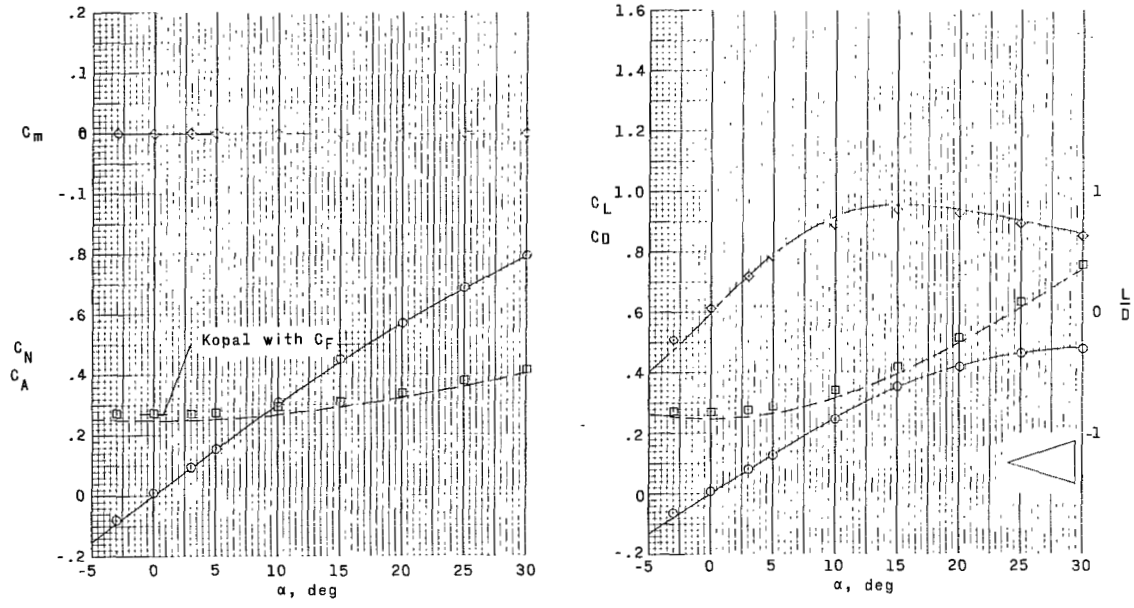

(a) $\theta = 20^\circ$; $R_\infty = 1.20 \times 10^6$.

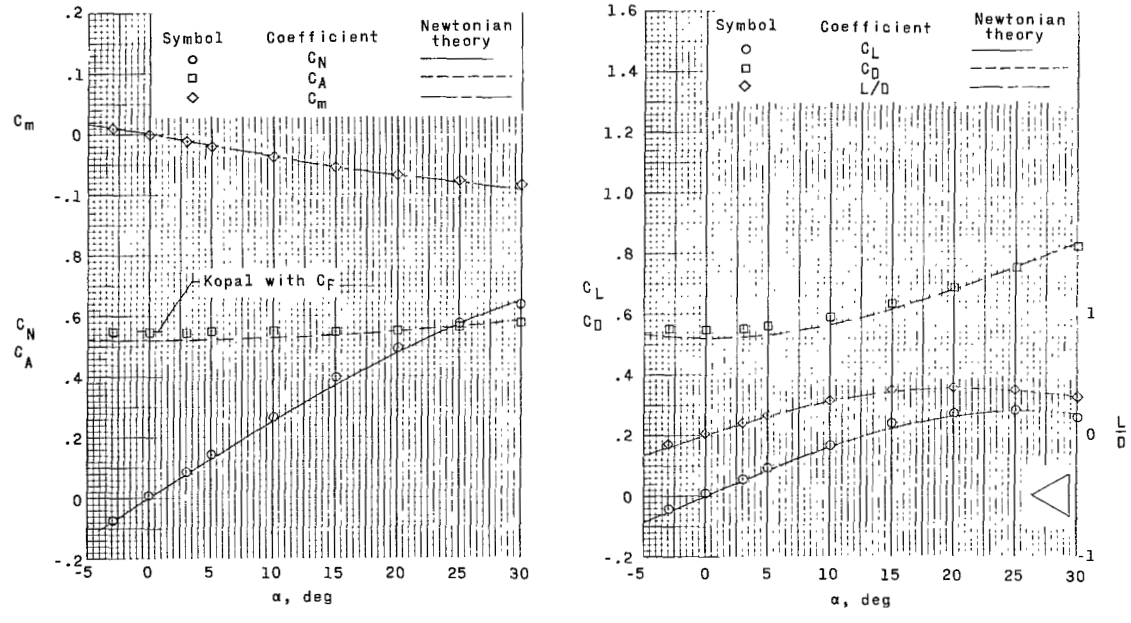

(b) $\theta = 30^\circ$; $R_\infty = 0.57 \times 10^6$.

Figure 5.- Comparison of longitudinal characteristics of cones having 20° and 30° semivertex angles with Newtonian theory. $M_\infty = 6.8$.

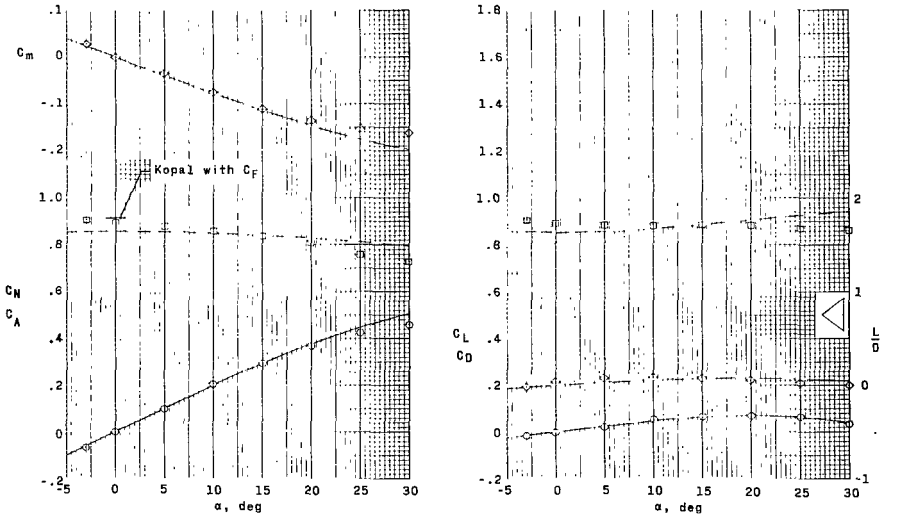

(a) $\theta = 40^\circ$; $R_\infty = 0.33 \times 10^6$.

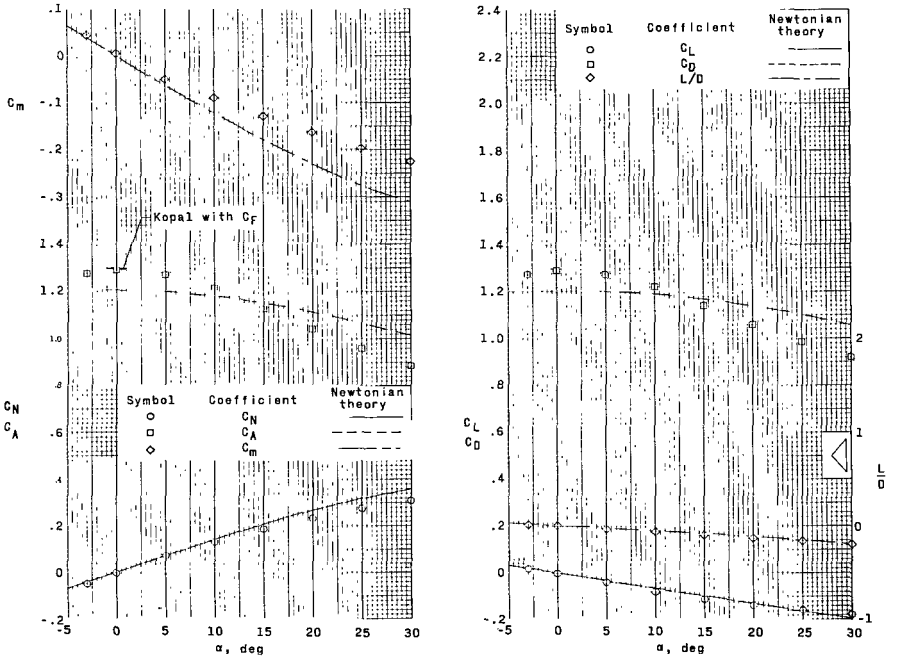

(b) $\theta = 50^\circ$; $R_\infty = 0.29 \times 10^6$.

Figure 6.- Comparison of longitudinal characteristics of cones having 40° and 50° semivertex angles with Newtonian theory. $M_\infty = 6.8$.

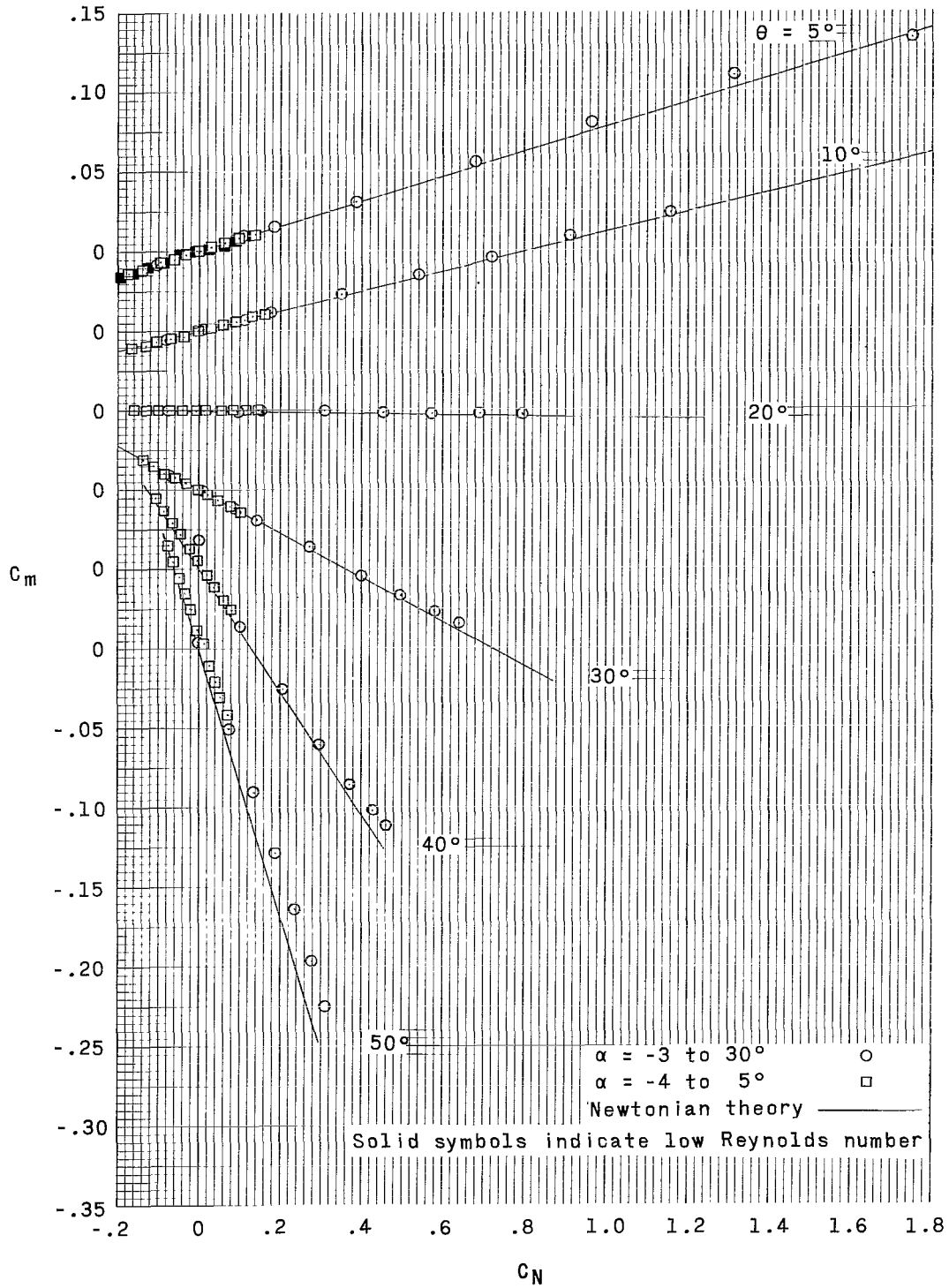

Figure 7.- Variation of pitching moment with normal force for various cones. $M_\infty = 6.8$.

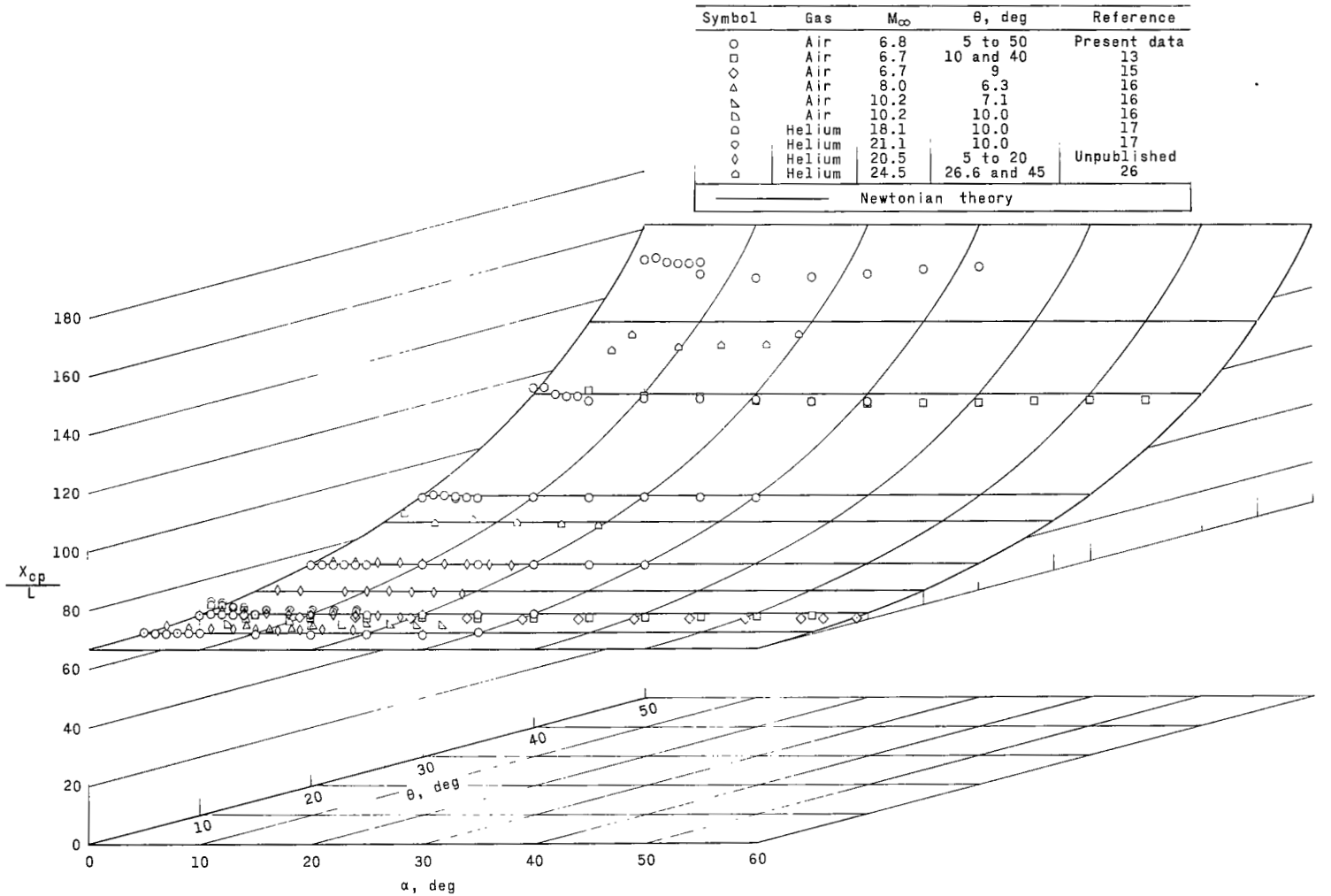

Figure 8.- Variation of the location of center of pressure with angle of attack and semivertex angle for various hypersonic Mach numbers.

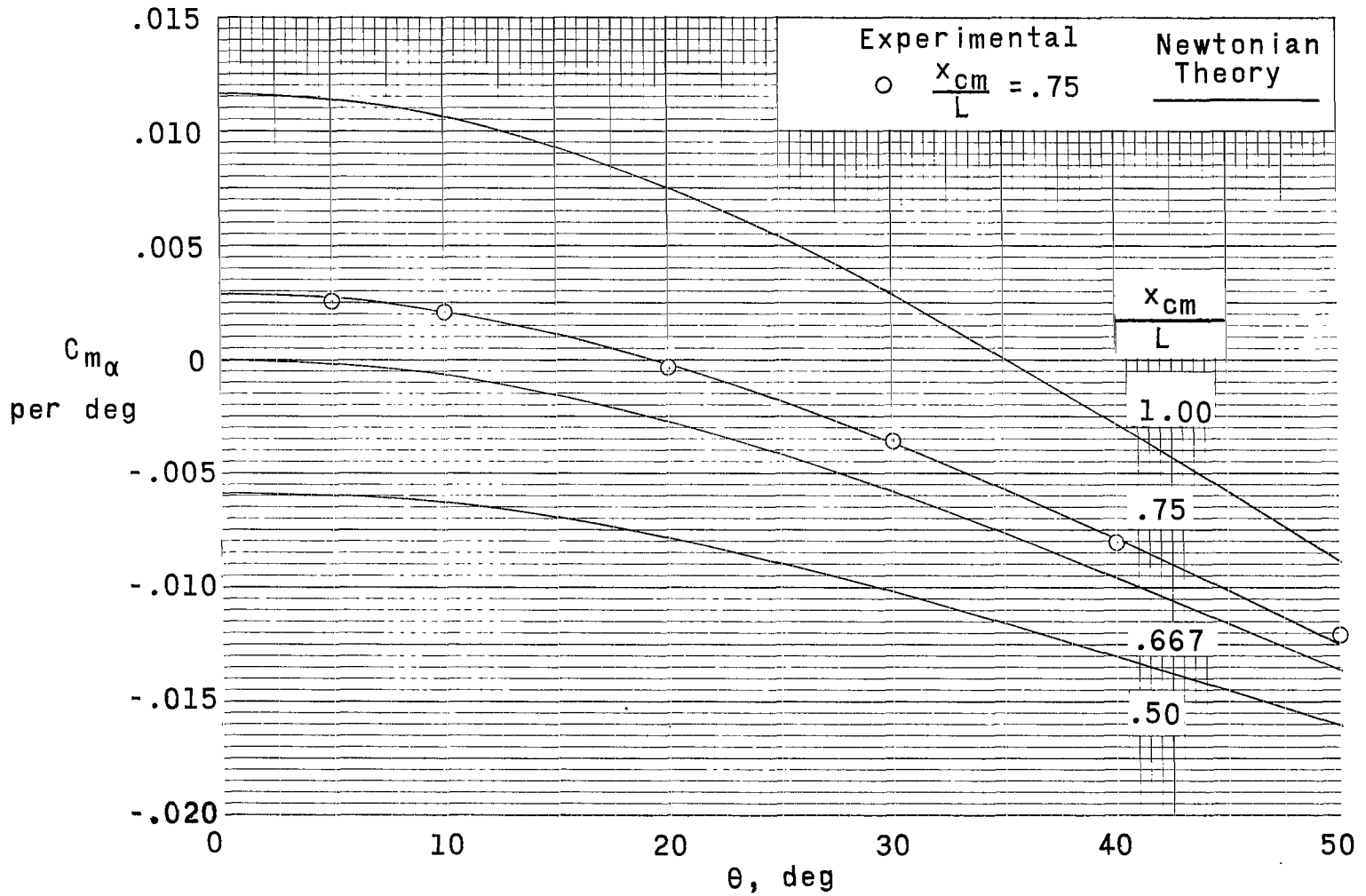

Figure 9.- Variation of static-stability parameter C_{m_α} with cone semivertex angle for various center-of-moment locations. $M_\infty = 6.8$.

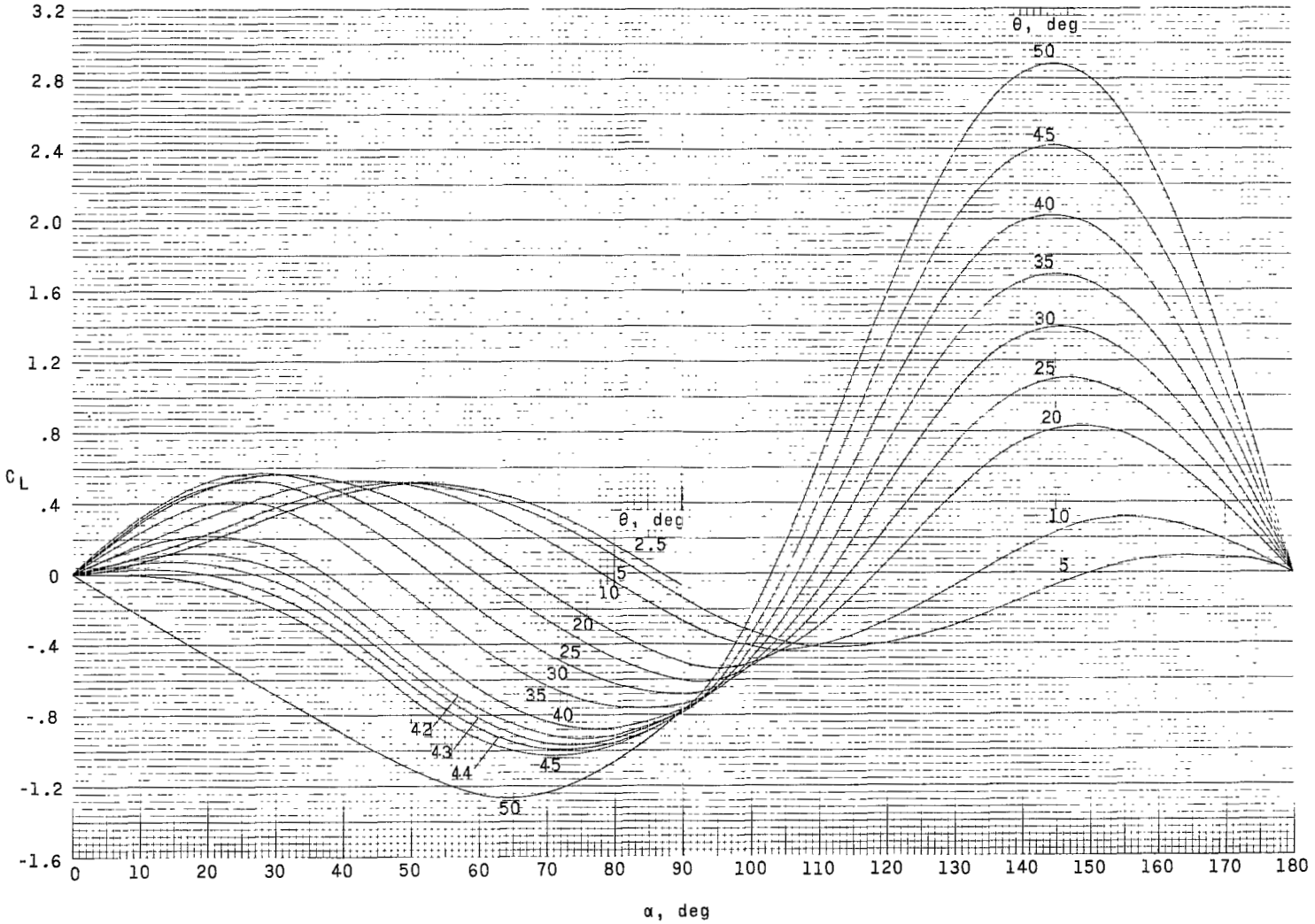

Figure 10.- Lift coefficients of various cones in Newtonian flow; $C_{p,max} = 2.0$. Coefficients referenced to planform area.

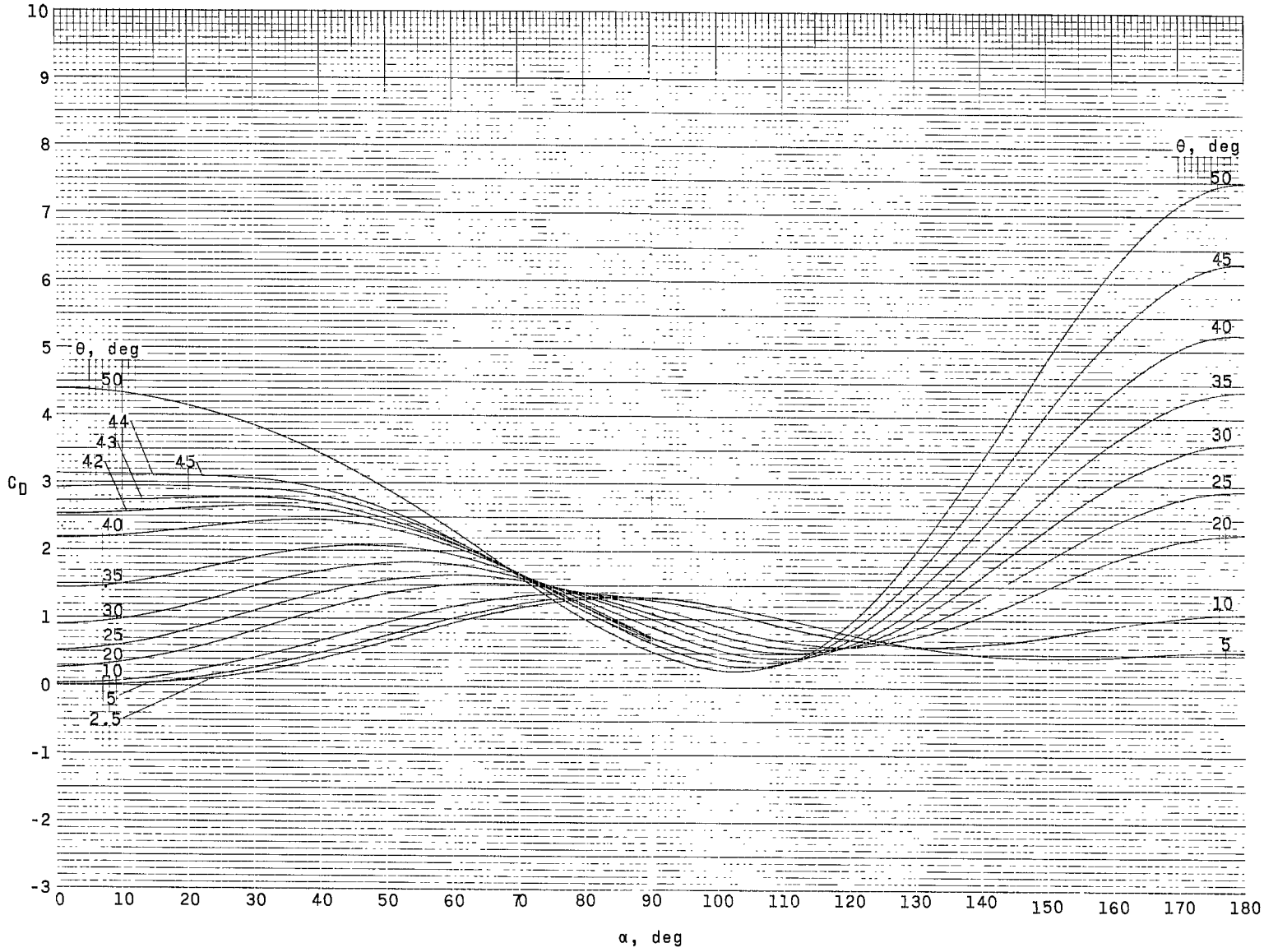

Figure 11.- Drag coefficients of various cones in Newtonian flow; $C_{p,max}$ = 2.0. Coefficients referenced to planform area.

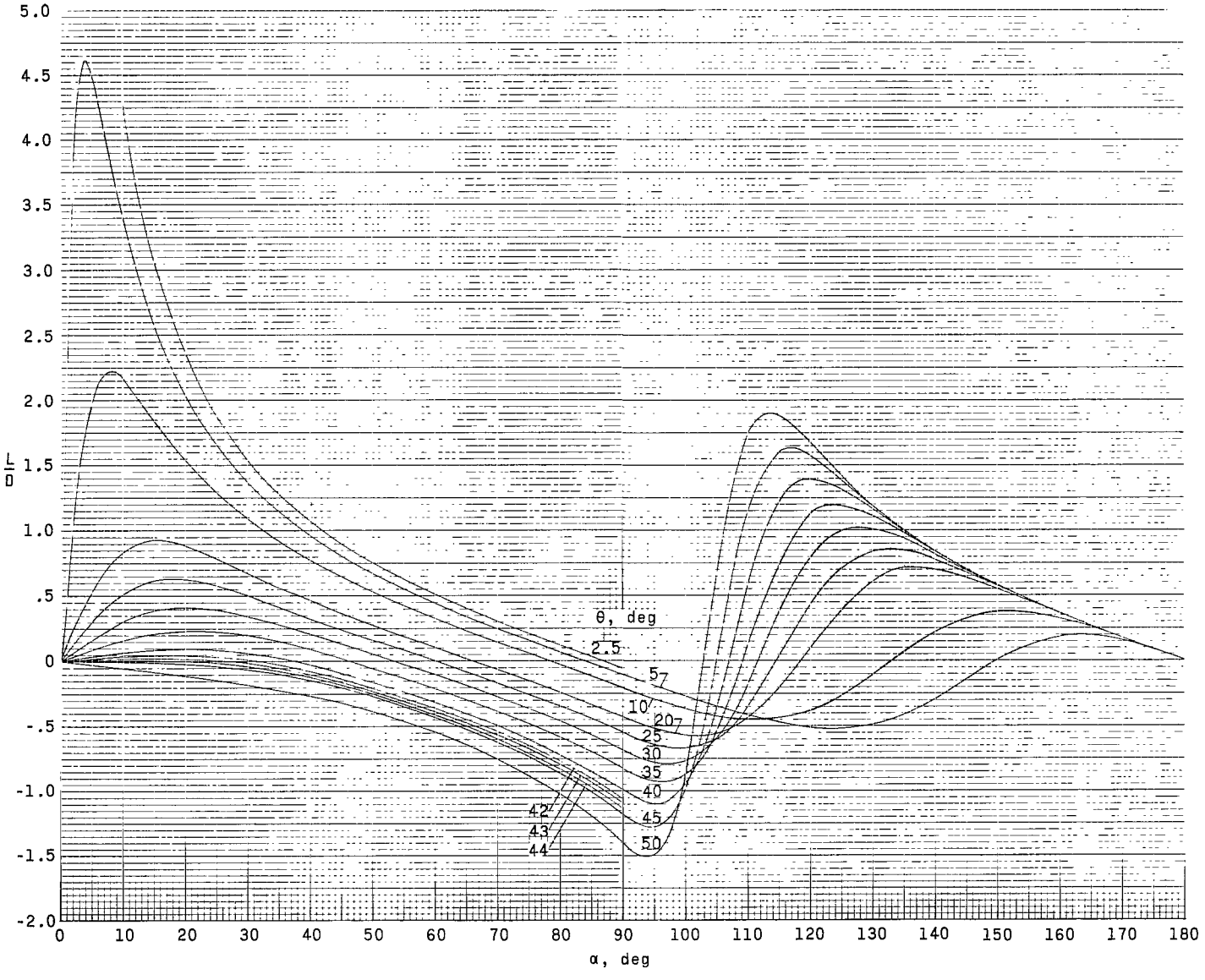

Figure 12.- Lift-drag ratio of various cones in Newtonian flow; $C_{p,max} = 2.0$.

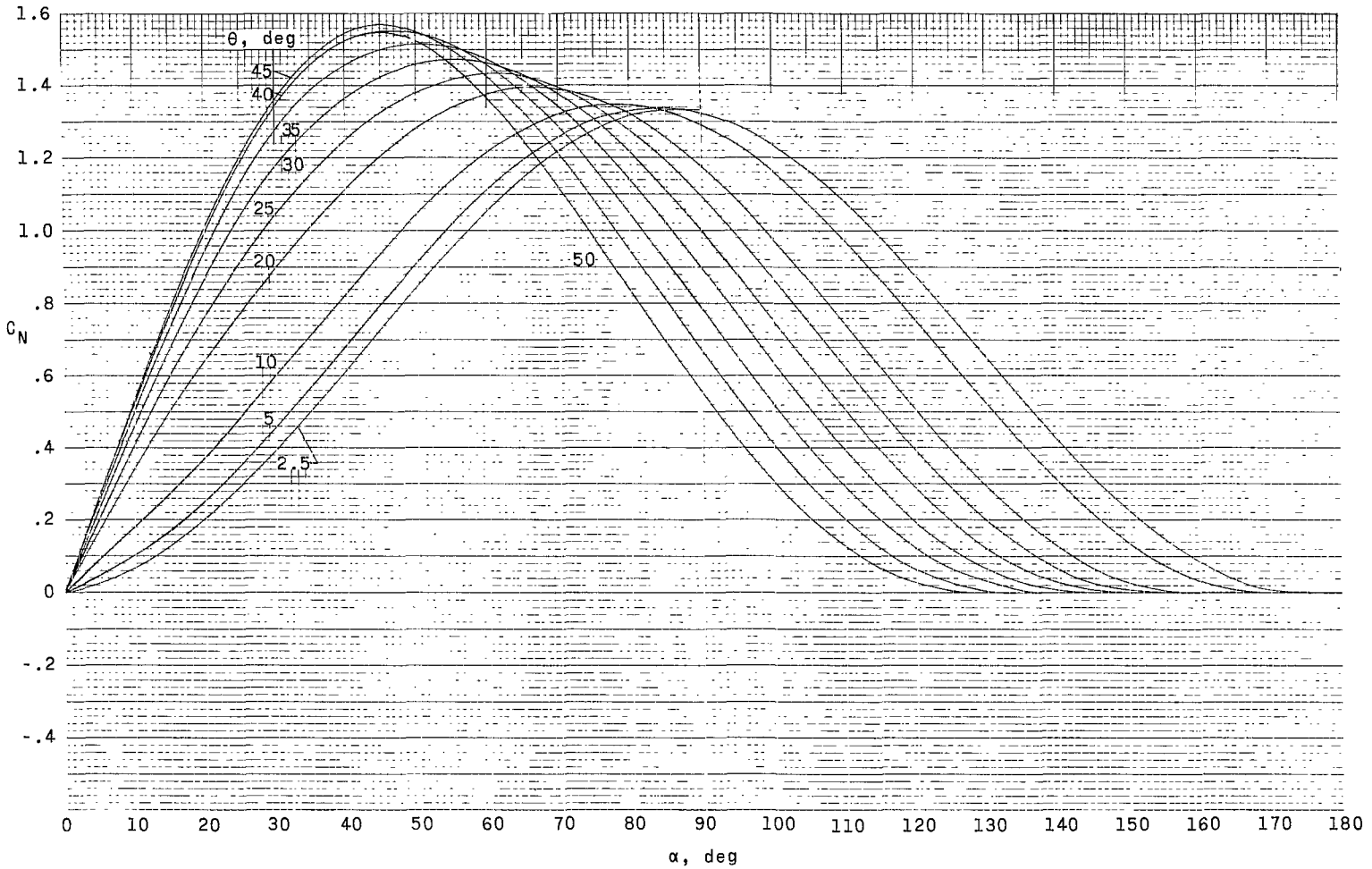

Figure 13.- Normal-force coefficients of various cones in Newtonian flow; $C_{p,max} = 2.0$. Coefficients referenced to planform area.

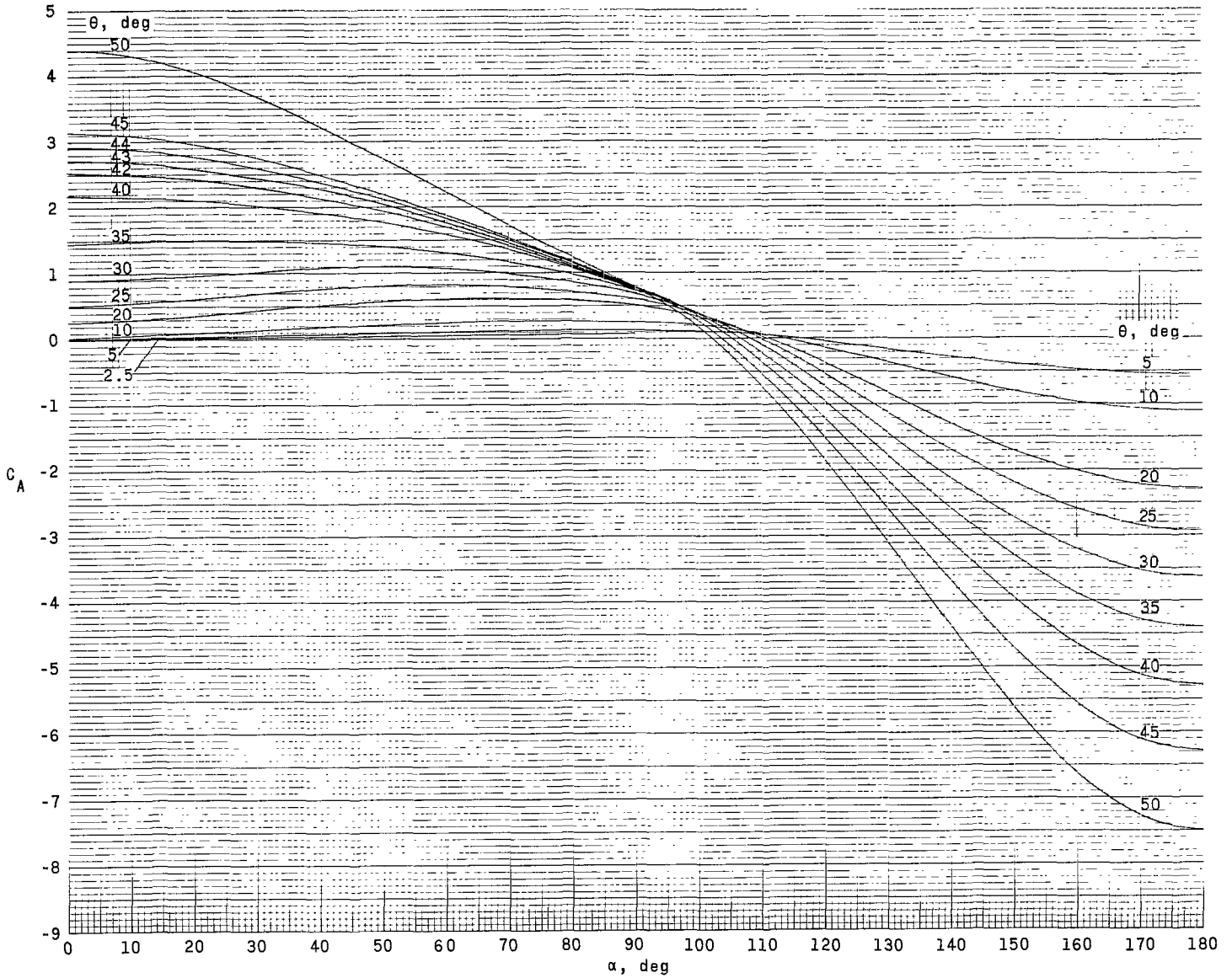

Figure 14.- Axial-force coefficients of various cones in Newtonian flow; $C_{p,max} = 2.0$. Coefficients referenced to planform area.

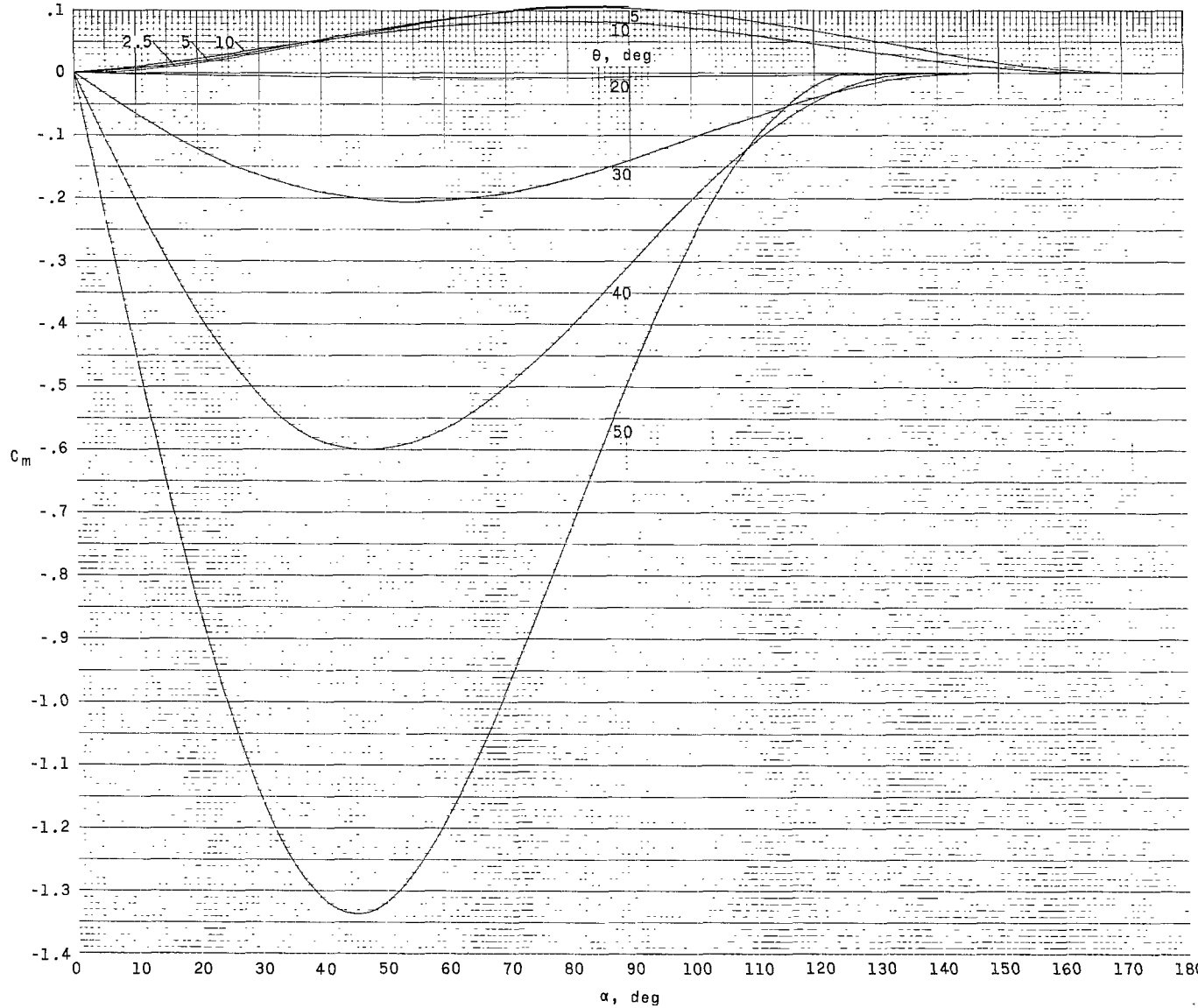

Figure 15.- Pitching-moment coefficients of various cones in Newtonian flow; $C_{p,max} = 2.0$. Coefficients referenced to planform area; center of moment at 0.75L.

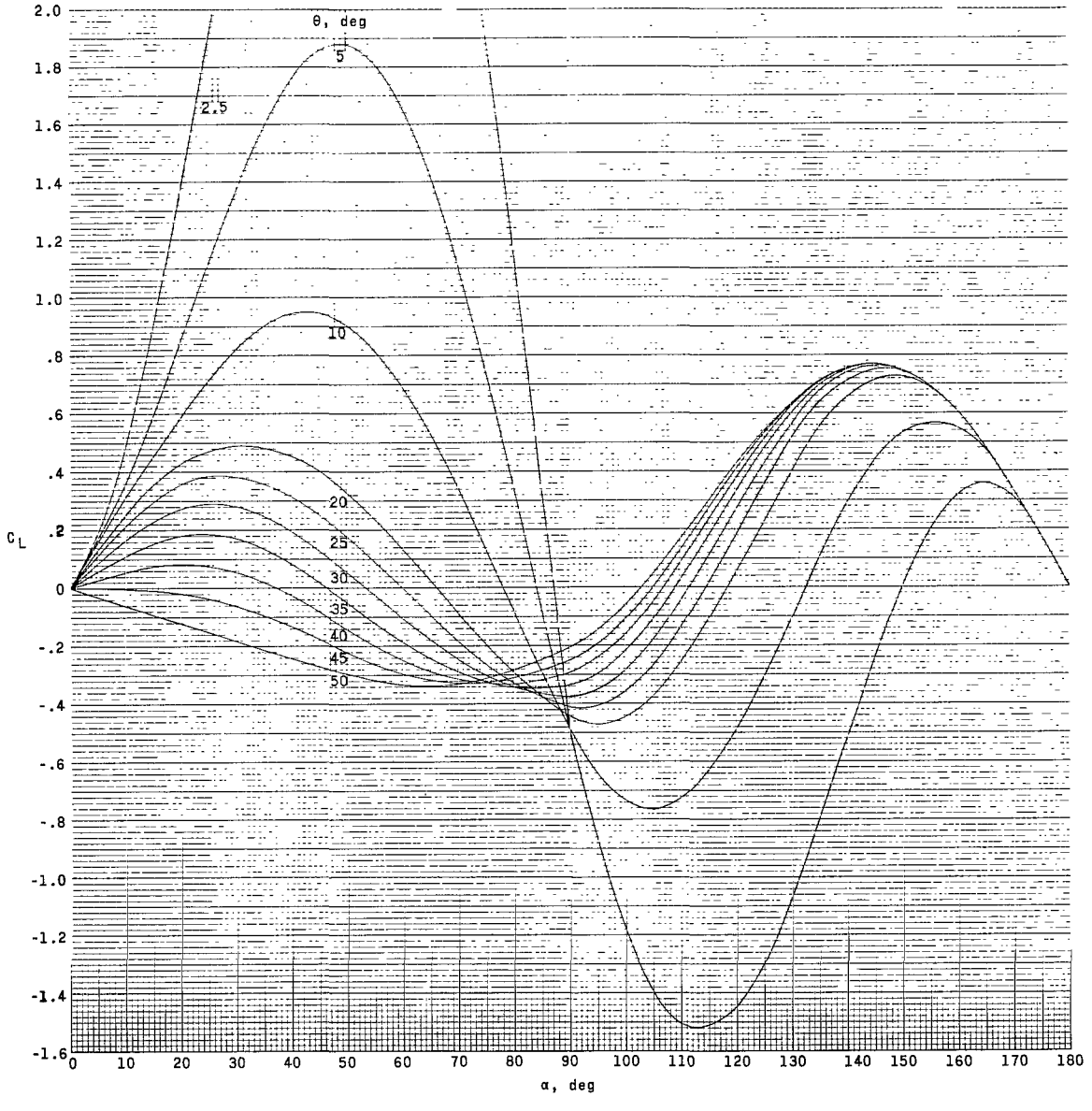

Figure 16.- Lift coefficients of various cones in Newtonian flow; $C_{p,max}$ = 2.0. Coefficients referenced to base area.

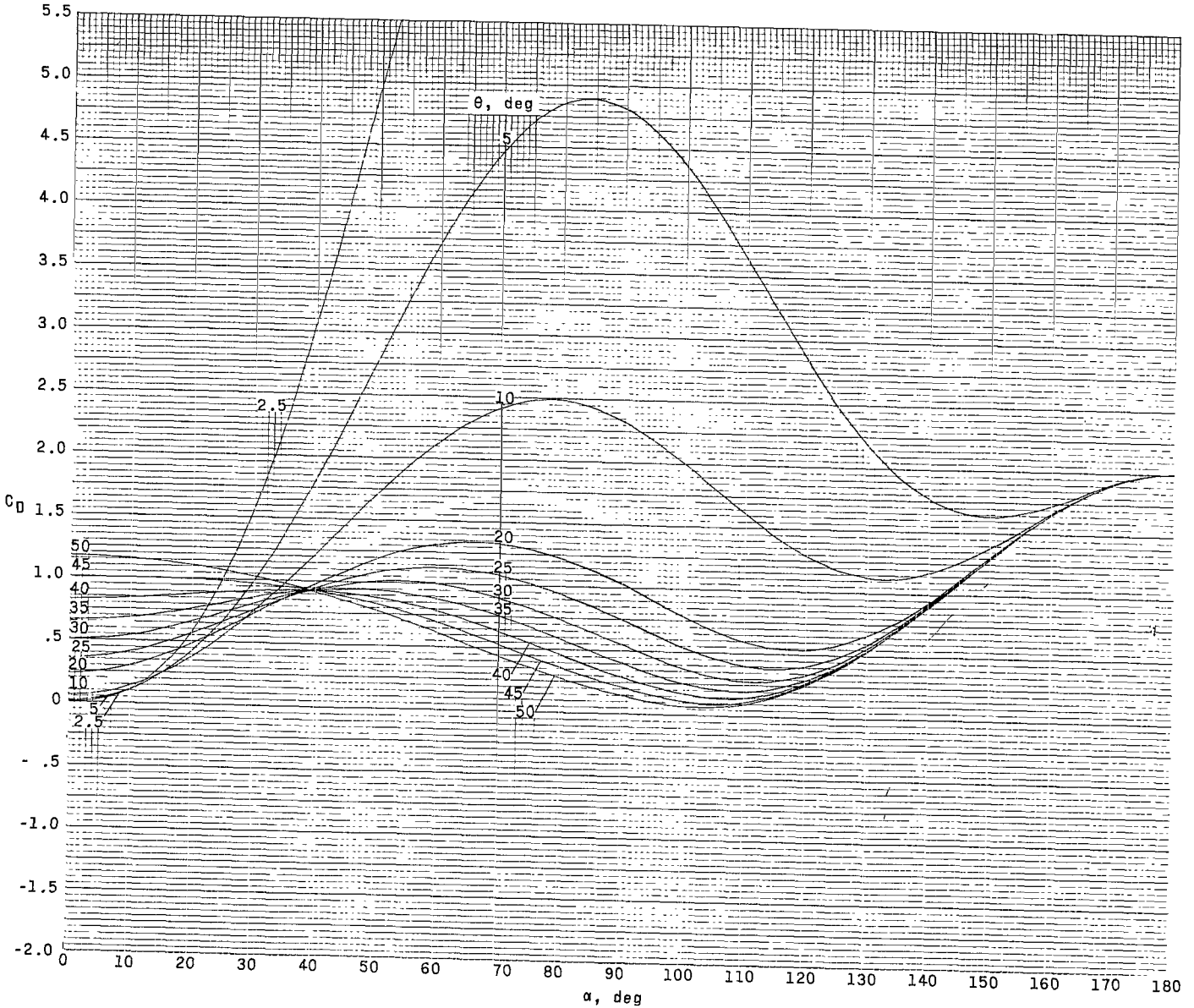

Figure 17.- Drag coefficients of various cones in Newtonian flow; $C_{p,max} = 2.0$. Coefficients referenced to base area.

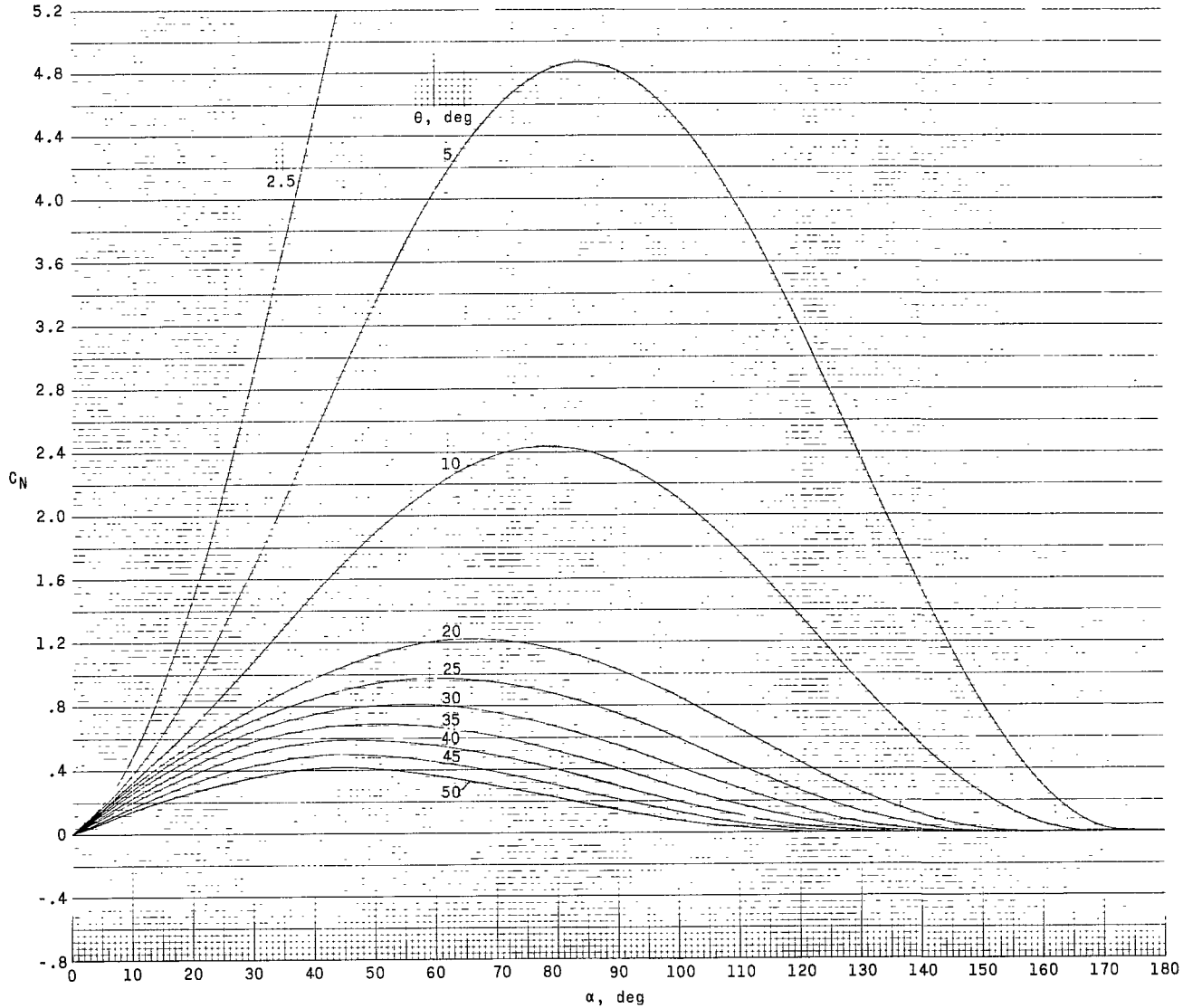

Figure 18.- Normal-force coefficients of various cones in Newtonian flow; $C_{p,max}$ = 2.0. Coefficients referenced to base area.

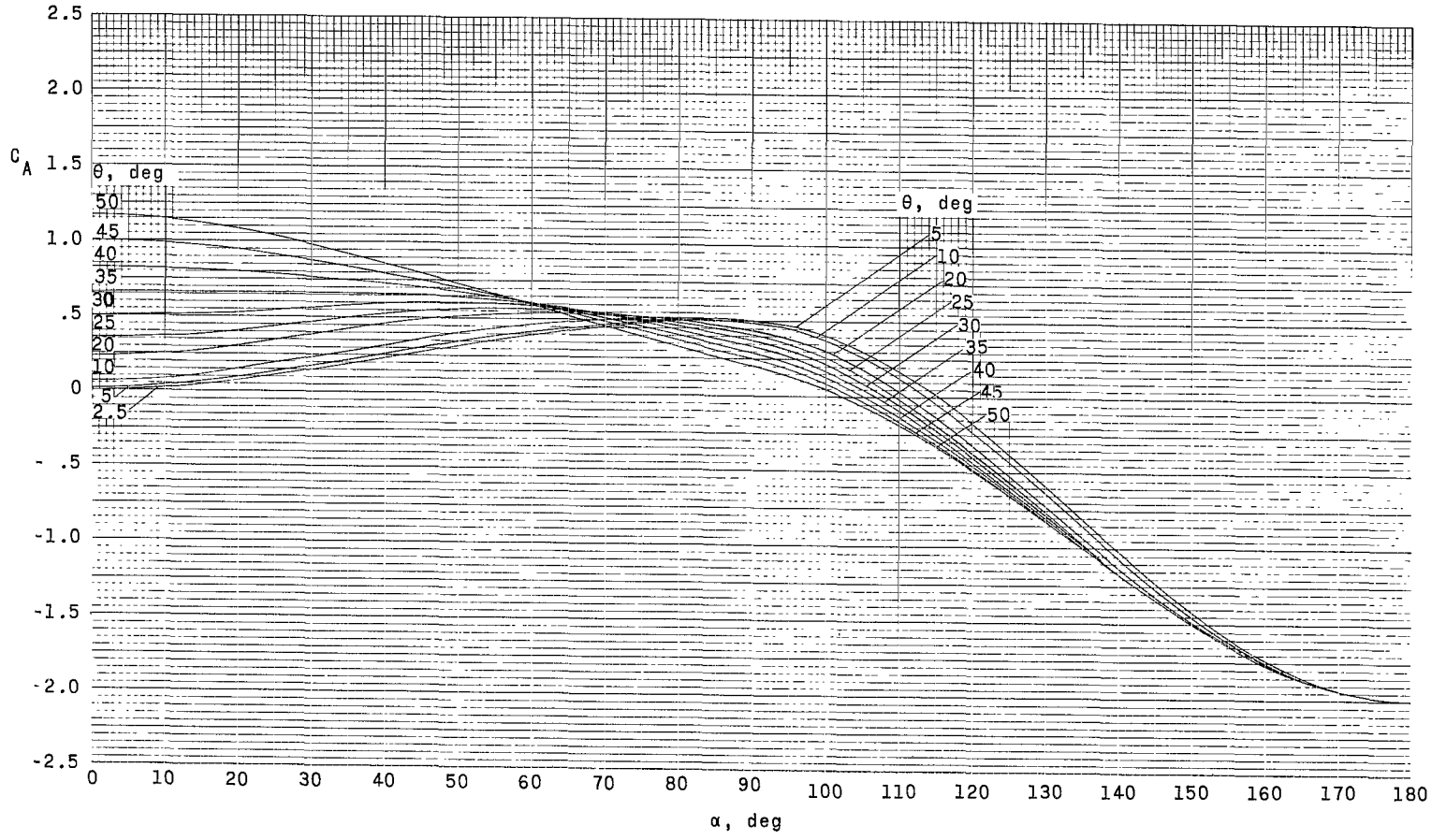

Figure 19.- Axial-force coefficients of various cones in Newtonian flow; $C_{p,max} = 2.0$. Coefficients referenced to base area.

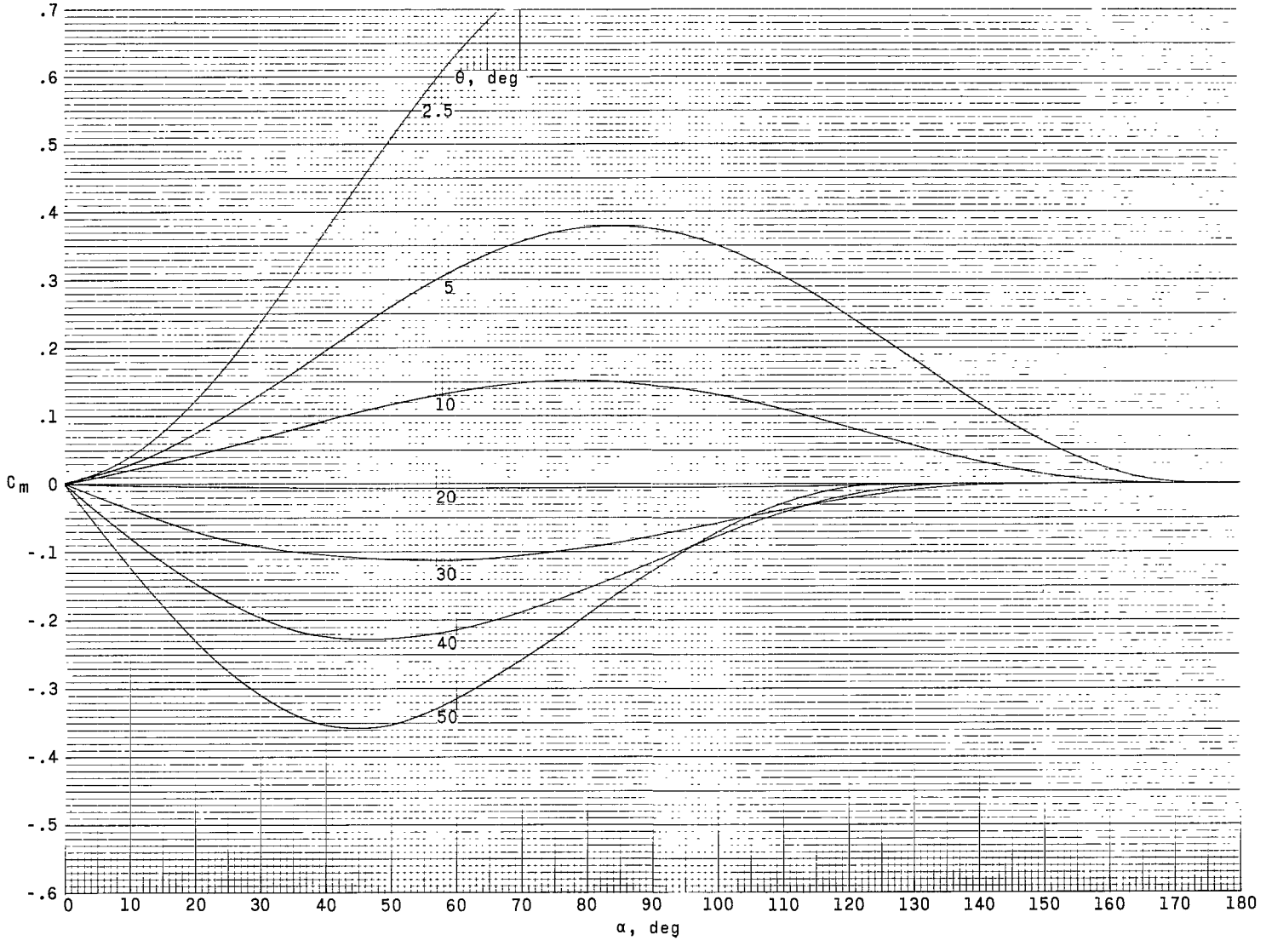

Figure 20.- Pitching-moment coefficients of various cones in Newtonian flow; $C_{p,max}$ = 2.0. Coefficients referenced to base area; center of moment at 0.75L.